Journal of the Geological Society, London, Vol. **161**, 2004, pp. 875–884. Printed in Great Britain.

Underplating-related finite-strain patterns in the Gran Paradiso massif, Western Alps, Italy: heterogeneous ductile strain superimposed on a nappe stack

OSAMA K. KASSEM & UWE RING

Institut für Geowissenschaften, Johannes Gutenberg-Universität, 55099 Mainz, Germany (e-mail: ring@uni-mainz.de)

Abstract: A finite-strain study in the central and northern Gran Paradiso massif of the Italian Western Alps has been carried out to elucidate whether ductile strain shows a relationship to nappe contacts and to shed light on the nature of the subhorizontal foliation typical of the gneiss nappes in the Alps. The R_f/φ and Fry methods were used on feldspar porphyroclasts from 98 samples of the Gran Paradiso unit (upper tectonic unit of the Gran Paradiso massif) and 12 samples from the underlying Erfaulet unit (lower unit of the Gran Paradiso massif). Microstructures and thermobarometric data show that feldspar ductility at temperatures higher than *c*. 450 °C occurred only during high-pressure metamorphism, when the rocks were underplated beneath the overriding Adriatic plate. Therefore, the finite-strain data can be related to high-pressure metamorphism in the Alpine subduction zone. The augen gneiss was heterogeneously deformed and axial ratios of the strain ellipse in *xz* sections range from 2.1 to 69.8. The long axes of the finite-strain ellipsoids trend west–WNW and the short axes are subvertical, associated with a subhorizontal foliation. The strain magnitudes do not increase towards the nappe contacts. The data indicate flattening strain type in the Gran Paradiso unit and constrictional strain type in the Erfaulet unit and prove deviations from simple shear. We conclude that nappe stacking occurred early during subduction probably by brittle imbrication and that ductile strain was superimposed on and modified the nappe structure during high-pressure underplating in the Alpine subduction zone. The accumulation of ductile strain during underplating was not by simple shear and involved a component of vertical shortening, which caused the subhorizontal foliation in the Gran Paradiso massif.

Keywords: Gran Paradiso massif, Western Alps, nappes, finite-strain analysis, shear.

A widely held opinion in tectonics is that nappe emplacement in orogens is by simple-shear deformation, which is a 2D constant-volume deformation that resembles the sliding of cards in a deck. A common feature of the interiors of the Pennine gneiss nappes in the Alps, and also of the internides of many other orogens, is that they have a penetrative subhorizontal foliation subparallel to tectonic contacts across their entire nappe thickness. In many cases, this foliation formed during thrusting of the nappes onto each other. Vertically oriented shortening causing subhorizontal foliations during nappe emplacement may result from a component of pure shear accompanying simple shearing or from simple shear with very high shear strains.

A number of finite-strain studies from natural shear zones show oblate geometries (Coward 1976; O'Hara 1990; Bailey *et al*. 1994; Ring 1999). These oblate fabrics may result from volume loss in simple shear zones or from a component of pure shear accompanying shearing with or without volume loss (Ramsay & Wood 1973; Simpson & De Paor 1993). A quantification of finite strain, the degree of non-coaxiality and volume strain is needed to evaluate the significance of such oblate strain geometries and how they are related to the flat-lying foliation characteristic of nappes in the internides of many orogens.

Other major problems include the stage of orogeny at which nappes form and what the relationship is between finite strain and nappe contacts. Common wisdom is that the bases of nappes are high-strain zones and that therefore the accumulation of large finite strains and nappe emplacement are intimately related. In the Alps, nappe contacts are, at least in part, major lithological boundaries and the occurrence of Permo-Mesozoic sediments between gneiss units is often used to map nappe boundaries (e.g. Spicher 1980). The contact between the oceanic Zermatt–Saas zone and the continental Gran Paradiso massif is also a major lithological boundary.

In this paper, the results of a finite-strain study in the northern and central Gran Paradiso massif of the Italian Western Alps are reported. The strain data show no obvious relationship to the nappe contacts, suggesting that ductile strain was superimposed on an already existing nappe structure. It is concluded that nappe stacking during high-pressure metamorphism in the Alpine subduction zone was not by simple shear alone and involved a component of pure shear, which is responsible for the subhorizontal foliation within the nappes.

Geological setting

The Western Alps form the north–south-striking part of the Alpine arc. They are characterized by regionally extensive outcrops of high-pressure rocks and offer the best possibility in the Alps to study the relationship between ductile strain and the nappe structure, which formed during subduction and high-pressure metamorphism (Schmid & Kissling 2000). The major lithotectonic units of the Western Alps are, from top to bottom: (1) the Austroalpine units; (2) the partly oceanic Pennine domain; (3) the Helvetic nappes (Fig. 1). The continental Austroalpine units can be separated into the Dent Blanche nappe and the Sesia zone (Ballèvre *et al*. 1986). The heterogeneous Combin zone marks the boundary between the Austroalpine units and the underlying Pennine nappes (Bearth 1956, 1976; Reddy *et al*. 1999). The Combin zone is separated from the underlying Zermatt–Saas zone by the Combin fault (Ballèvre & Merle 1993; Ring 1995). The Zermatt–Saas zone is a South Pennine oceanic unit made up of serpentinite, metagabbro, metabasalt, metachert and Bündnerschiefer (Bearth 1976). The continental

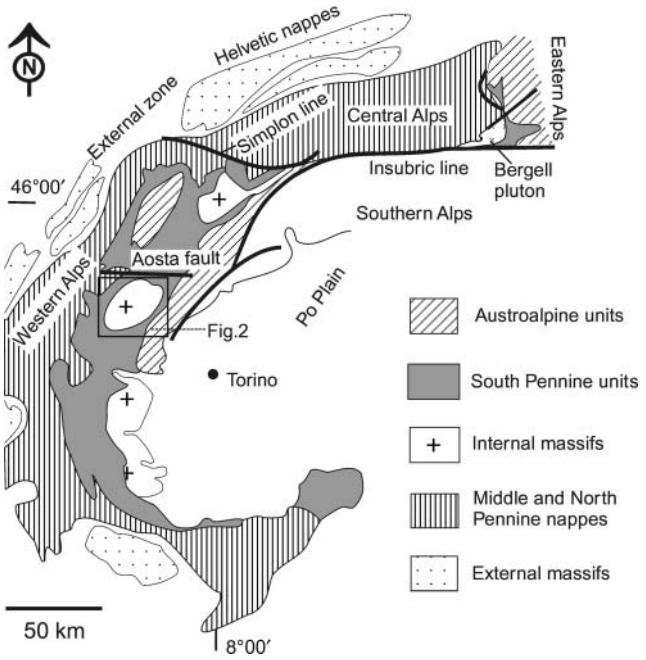

Fig. 1. Tectonic sketch map of the Western and Central Alps (box shows location of Fig. 2).

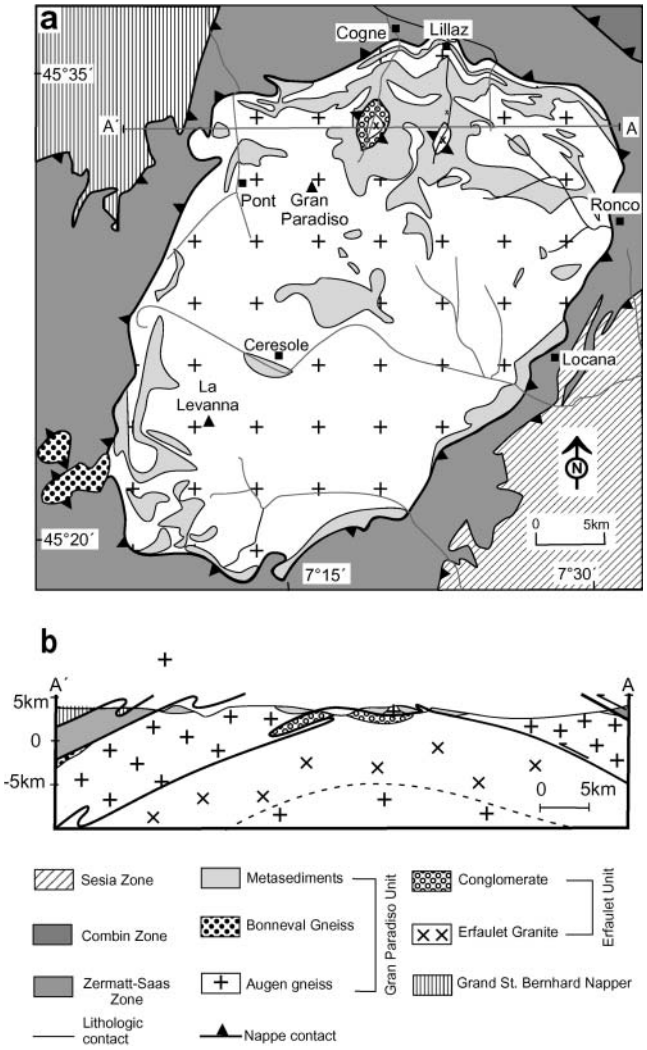

Fig. 2. (**a**) Tectonic map of the Gran Paradiso massif; cross-section A–A′ and major streams (fine black lines) are indicated. (**b**) Cross-section A–A′ showing broad domal structure; the Erfaulet unit forms the base of the exposed section and crops out in major valleys; west-vergent folding in central part of section is overprinted by late-stage backfolding in the western part of section.

basement of the Gran Paradiso massif occurs below the Zermatt–Saas zone. It has the same Middle Pennine tectonic position as the Monte Rosa nappe, Dora Maira massif and the more externally outcropping Grand St. Bernard nappe (Ballèvre *et al*. 1986). Because the Gran Paradiso massif, the Monte Rosa nappe and the Dora Maira massif form windows within the South Pennine oceanic units, they are regarded as internal massifs. The North Pennine Sion–Courmayeur zone was thrust over the Helvetic zone along the Pennine thrust (Ceriani *et al*. 2001).

In this paper we focus on the Gran Paradiso massif (Fig. 2a), which consists of two subunits. The first is the upper Gran Paradiso unit made up of pre-Permian metasediments, into which the granitic precursor of a widespread augen gneiss was intruded in the Carboniferous (Compagnoni & Prato 1969; Compagnoni *et al*. 1974), and also remnants of a Permo-Mesozoic cover. The metasediments form a thin blanket at the top of the Gran Paradiso unit. It seems that the contact between augen gneiss and metasediments represents a strong mechanical anisotropy along which the basal thrust of the Zermatt–Saas zone developed. The second subunit is the tectonically lower Erfaulet unit, which comprises metaconglomerate, metapelite and metagranite–augen gneiss. Compagnoni *et al*. (1974) suggested a Late Carboniferous and/or Permian age for the conglomerate. In the southwestern part of the Gran Paradiso massif, the Bonneval gneiss crops out above the augen gneiss of the Gran Paradiso unit (Vearncombe 1985). It is a commonly mylonitic, banded gneiss derived from Permian volcanic rocks and sediments (Bertrand 1968) and is therefore part of the Permo-Mesozoic cover of the Gran Paradiso unit. The Bonneval gneiss is separated from the augen gneiss by a fault zone in which dolomite, cargneule, anhydrite and Bündnerschiefer occur (Bois & Fabre 1956). The penetrative foliation in the Gran Paradiso massif is generally flat-lying and forms a broad structural arch (Fig. 2b).

Borghi *et al*. (1994, 1996) and Borghi & Sandrone (1996) showed that the pre-Permian metasediments of the Gran Paradiso unit were first metamorphosed and deformed during the Variscan orogeny, whereas the rocks of the Erfaulet unit were not affected by the Variscan orogeny. Detailed work by Borghi *et al*. (1994) showed that during the Alpine orogeny, maximum metamorphic conditions of both units were different: peak P–T conditions of the Gran Paradiso unit were 12–14 kbar and 500–550 °C, whereas high-pressure metamorphism of the Erfaulet unit occurred at 11–13 kbar and 450–500 °C. The metamorphic evolution after the high-pressure overprint was similar in both units, indicating that they were juxtaposed during and/or soon after the peak of high-pressure metamorphism. There are no data constraining the age of high-pressure metamorphism or associated deformation in the Gran Paradiso massif. Sm–Nd data for pyrope and the U–Pb ages for zircon from the correlative Dora Maira massif have been interpreted to date the high-pressure event at 38–40 Ma (Tilton *et al*. 1991). Zircon and apatite fission-track ages of *c*. 30 Ma and 24–19 Ma, respectively

(Hurford & Hunzikar 1989), indicate cooling after the greenschist-facies overprint in the Gran Paradiso massif.

Methods of strain analysis

To quantify finite strain, the R_f/φ and Fry techniques (Ramsay 1967; Fry 1979; Ramsay & Huber 1983) were used. Feldspar grains from augen gneiss of the Gran Paradiso unit (94 samples) and the Erfaulet granite (nine samples) and quartzite pebbles from conglomerates of the Permo-Mesozoic cover of the Gran Paradiso (four samples) and the Erfaulet (three samples) units were analysed by the R_f/φ method. The Fry method was applied to seven samples to compare the results with those obtained by the R_f/φ method. Feldspar grains from one metasediment sample were also analysed by the Fry method to see whether the strain recorded in the metasediments is of the same magnitude as those in augen gneiss and conglomerate. Two-dimensional strain measurements were made on *xy*, *xz* and *yz* sections ($x \geqslant y \geqslant z$, finite-strain axes) to estimate the 3D strain geometry. A least-squares best-fit ellipse was calculated for each marker outline as well as its relative position and orientation. For R_f/φ analysis on feldspar, the long and short axes of up to 40 grains per section were measured and mean aspect ratios for each section were calculated. Tectonic strains were determined from the χ^2 minima of the R_f/φ analyses (Peach & Lisle 1979). For Fry analysis, the central points of more than 100 feldspar grains per section were used to calculate strain. The strain estimates were used to calculate the finite-strain ellipsoid according to the modified least-squares technique of Owens (1984). The Nadai strain magnitude is defined by an orthogonal coordinate system using the natural principal strains *Ex*, *Ey* and *Ez* (Ramsay & Huber 1983). The distance from the origin provides an invariant measure of the total strain magnitude (E_t), which can be separated into two orthogonal components: volume (E_v) and deviatoric (E_d) strain ($E_t = (E_d^2 + E_v^2)^{1/2}$). E_v and E_d are independent of the rotational component of deformation.

To investigate the possibility of deformation-related volume change, major oxide and trace element concentrations were plotted on isocon diagrams (Grant 1986). These diagrams compare element concentrations in the altered rock (mylonite) with concentrations in the original rock (protolith). The basic argument is that some components are likely to have been immobile in the alteration process and, for example, should be relatively enriched in mylonite that underwent volume loss (O'Hara & Blackburn 1989). If these elements can be identified, volume change can be calculated assuming that the volume change is a factor common to the behaviour of all components. During regional deformation, Al, Ti and Zr are usually immobile. The experimental results of Ayers & Watson (1991) indicated that rutile and zircon solubilities and solubility gradients in high-grade P–T fields will be extremely low for typical water-rich fluid compositions. If significant mobility of Ti and Zr took place during metamorphism, then it is likely that rutile and zircon would have grown in veins, which has never been observed in and next to the sample localities.

Major- and trace-element analyses were performed by standard XRF spectroscopy, using glass fusion discs and pressed powder pellets. All analyses were made with a sequential Philips PW 1404 wavelength-dispersive XRF system with excitation by an Rh X-ray tube. Operating conditions were between 40 and 80 kV and 30 and 60 mA, depending on the element analysed.

Data

Deformation structures

The structure of the area is dominated by a pervasive, subhorizontal main-phase foliation (Figs 3 and 4). The main-phase

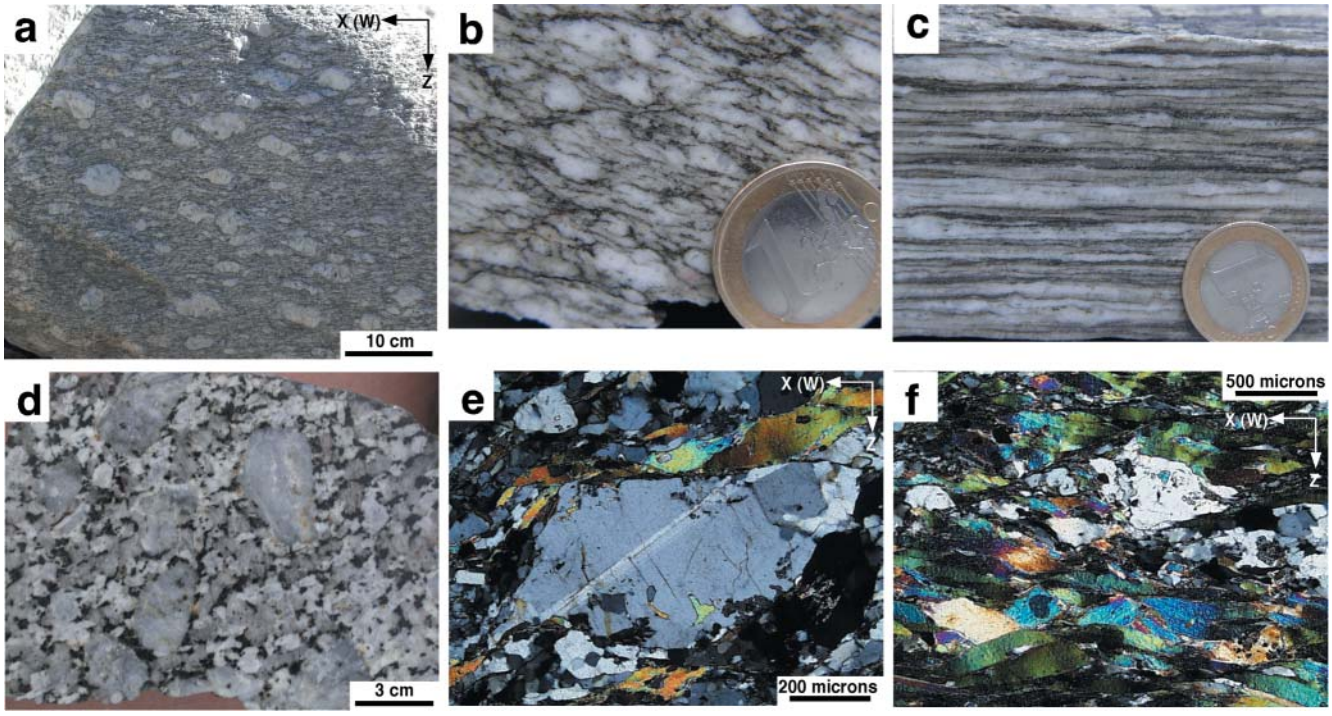

Fig. 3. (**a**) *xz* section of moderately deformed augen gneiss SSE of Pont (note augen structure). (**b**) Deformation and recrystallization of feldspar resulting in elongated feldspar grains; augen structure is still preserved; sample GP02-109. (**c**) Mylonitic deformation of augen gneiss leading to platy gneiss; sample GP02-106. (**d**) Weakly deformed metagranite east of Ceresole; large feldspar clasts are at a high angle to foliation. (**e**) Dynamically recrystallized feldspar porphyroclasts; sample GP02-80A. (**f**) Recrystallized feldspar porphyroclasts and mica fish indicating top-to-the-west shear sense; sample GP02-102.

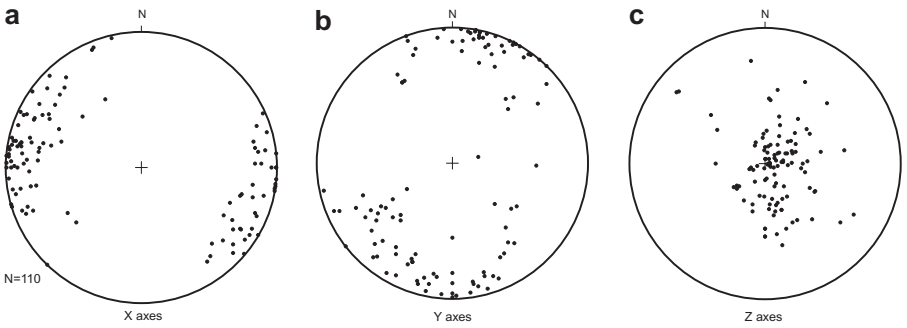

Fig. 4. Lower-hemisphere equal-area projections of principal strain directions; *x* axes show a strong maximum in a WNW–ESE direction; *z* axes reflect the subhorizontal foliation.

foliation is subparallel to the nappe contact of the Gran Paradiso massif with the overlying Zermatt–Saas zone and defines a broad regional dome structure. Vissers & Compagnoni (1984) showed that the main-phase foliation cuts the tectonic contact between the Gran Paradiso unit and the Erfaulet unit at a low angle. This observation is important because it indicates that nappe stacking started before major deformation. Vissers & Compagnoni workers argued that the Gran Paradiso massif is a gneiss-cored fold nappe with the Erfaulet unit occurring in the axial plane of the fold nappe (see also Schmid & Kissling 2000).

The augen gneiss of the Gran Paradiso unit is very heterogeneously deformed in the field (Fig. 3). Localities where feldspar grains in platy gneiss are extremely smeared out with aspect ratios >25 in *xz* sections (and feldspar augen no longer exist), laterally and vertically grade over short distances of *c*. 100 m into moderately deformed augen gneiss (showing a distinct augen structure) (Fig. 3a) with *xz* aspect ratios of 3–4. The development of an augen gneiss fabric appears to be controlled by moderate deformation of a formerly porphyritic granite, whereas intense deformation destroyed any former porphyritic or augen fabric (Fig. 3b and c). However, the platy gneiss does not characterize the nappe contact of the Gran Paradiso unit with the Zermatt–Saas zone. We studied this nappe contact in detail near Cogne and Lillaz (Fig. 2). Augen gneiss and quartzite conglomerate there typically have clasts with aspect ratios of 2–6 in *xz* sections. Close to the contact of the Gran Paradiso unit with the Zermatt–Saas zone near Ronco, well-preserved intrusive relationships of the granite precursor of the augen gneiss into metapelite are abundant (see also Callegari *et al*. 1969). In the structurally lower parts of the Gran Paradiso unit east of Ceresole in the central massif, augen gneiss appears almost undeformed (Fig. 3d). At the contact of the augen gneiss unit with the Erfaulet unit south of Cogne and south of Lillaz, the augen gneiss also does not appear strongly deformed.

In the augen gneiss, the main-phase foliation is a gneissic layering defined by elongated, dynamically recrystallized feldspar porphyroclasts, myrmekite growth and alignment of mica and quartz (Fig. 3e and f). In the metasedimentary rocks of the Gran Paradiso unit, the morphology of the foliation varies from a differentiated layering, with relics of crenulations in quartz-rich microlithons, to a pervasive schistosity. Vissers & Compagnoni (1984), Vearncombe (1985) and Borghi *et al*. (1994) showed that the main-phase foliation is superimposed on an earlier Alpine foliation.

On the main-phase foliation, a west- to WNW-trending stretching lineation is developed (Figs 4 and 5). In augen gneiss, this stretching lineation is well expressed by the alignment of recrystallized tails around feldspar porphyroclasts and preferred orientation of quartz and mica aggregates. In metasedimentary rocks, strain shadows around garnet and quartz–mica alignment define the stretching lineation. Asymmetric strain shadows around garnet and shear bands indicate top-to-the-west or -WNW shear (Fig. 3f). Strain shadows around feldspar porphyroclasts contain recrystallized potassium feldspar, plagioclase and quartz. Assumed temperatures for the onset of ductility of potassium feldspar are usually of the order of >450–500 °C (Voll 1980; Pryer 1993).

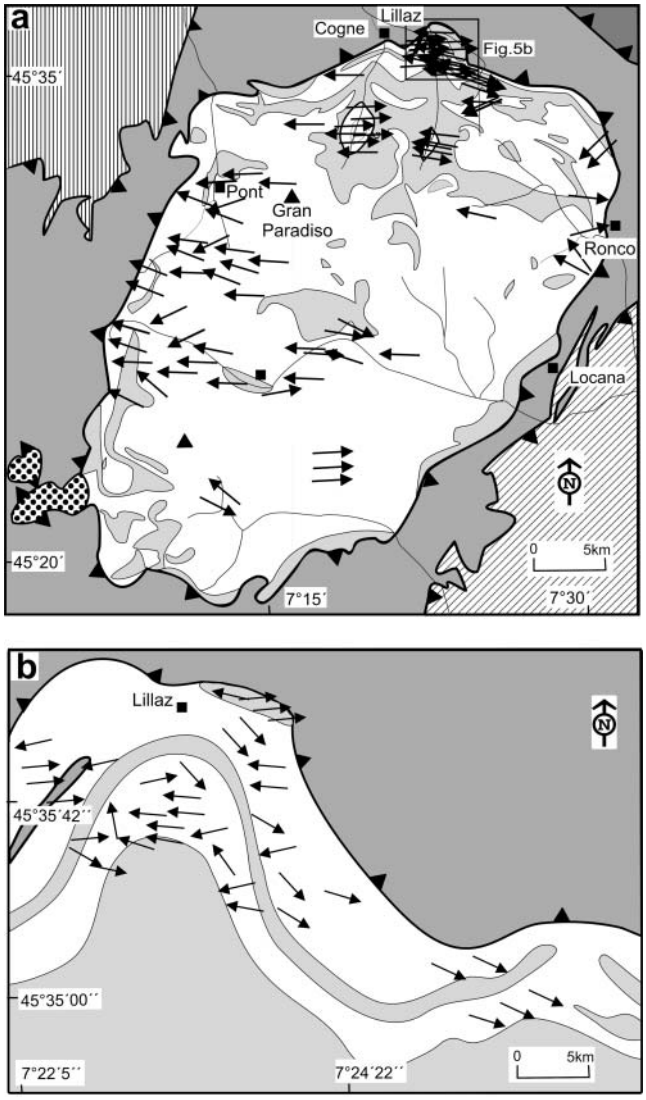

Fig. 5. (**a**) Lineation map for the Gran Paradiso massif and (**b**) the contact between the Gran Paradiso massif and the Zermatt–Saas zone near Lillaz; arrowheads indicate plunging direction.

The main-phase foliation and stretching lineation were deformed by two subsequent deformation events during greenschist- to sub-greenschist-facies metamorphism (Vissers & Compagnoni 1984; Vearncombe 1985; Butler & Freeman 1996). The latest of these deformation events is associated with localized top-to-the-east or -ESE shearing. It is important to note that potassium feldspar did not deform in a ductile fashion during post-peak-metamorphic deformation.

Results of finite-strain analysis

The sample localities for finite-strain analysis are shown in Figure 6, and the complete set of finite-strain data can be obtained from the Society Library or the British Library Document Supply Centre, Boston Spa, Wetherby, West Yorkshire LS23 7BQ, UK as Supplementary Publication No. SUP 18204 (4 pages). It is also available online at http://www.geolsoc.org.uk/SUP018204. The strain data are shown in a Flinn diagram in Figure 7a. The Flinn diagram shows the relative shapes of the strain ellipsoids, i.e. prolate v. oblate. According to Hossack (1968), this classification is called strain symmetry. To infer strain type, i.e. constrictional v. flattening, information on volume strain is needed.

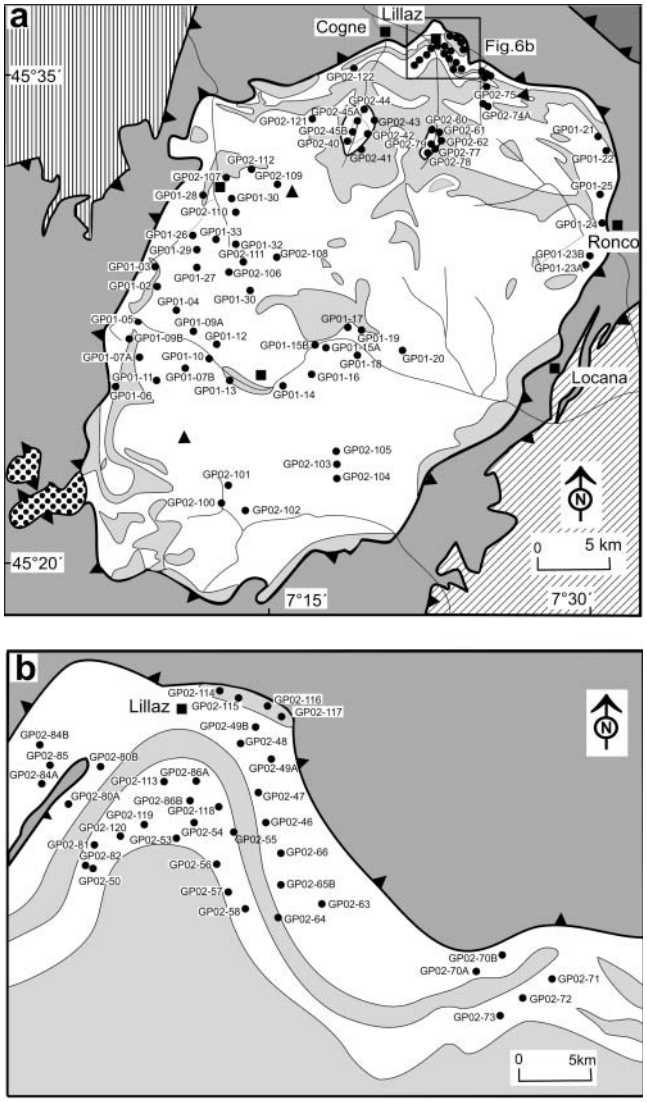

Fig. 6. (**a**, **b**) Maps showing localities of finite-strain samples.

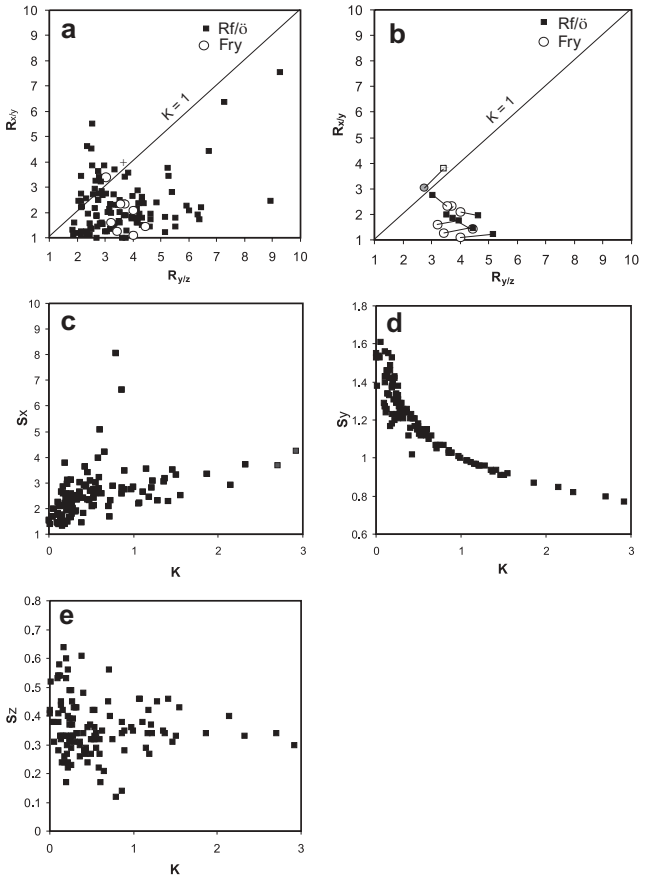

Fig. 7. (**a**) Flinn diagram showing relative strain or strain symmetry as obtained by R_f/φ (■) and Fry (○) analysis. (**b**) R_f/φ and Fry data from the same samples connected by tie-lines; grey sample points show data from metasediment. (**c**) *Sx* v. *K* showing positive correlation. (**d**) *Sy* v. *K* showing pronounced negative correlation. (**e**) *Sz* v. *K* depicting no obvious correlation.

To prove that strain analysis by the R_f/ϕ method yields meaningful results, one has to demonstrate that the measured objects deformed largely homogeneously with their matrix. Finite strains determined with the normalized Fry technique were primarily used to check the R_f/ϕ estimates. The Fry strains are thought to represent the matrix strain, whereas the R_f/ϕ strains describe the fabric ellipsoid or clast strain (Ramsay & Huber 1983; Ring 1998). As shown in Figure 7b, Fry strains are not fundamentally different from R_f/ϕ strains; in most cases, the R_f/ϕ strains are slightly greater than the Fry strains, but in other cases the opposite is the case. Therefore, we conclude that there was no significant competence contrast between the quartz–mica matrix and the feldspar porphyroclasts during the accumulation of finite strain at peak metamorphic conditions. Furthermore, finite strain in the augen gneiss is of the same order of magnitude as those obtained from the conglomerate and metasediment samples. The main-phase foliation is not refracted between augen gneiss and metasediments, which also suggests similar deformation behaviour in both lithologies. Hence, R_f/ϕ strains derived from analysing feldspar porphyroclasts are representative for regional strain at peak metamorphism.

In general, the strain ellipsoids have oblate strain symmetry

with some data points in the prolate field (Fig. 7a). The axial ratios in *xz* sections range from 2.10 to 69.81 with *Sx* ranging from 1.40 to 8.08. The stretches in the *z* direction, *Sz*, range from 0.12 to 0.64, indicating strong vertical shortening of 36–88%. *Sy* ranges from 0.77 to 1.56, showing both contraction and extension in this direction. The strain data verify the pronounced heterogeneous deformation of the augen gneiss observed in the field.

The amount of strain as defined by the Nadai strain magnitude has been plotted for all samples on two maps (Fig. 8) and the strain magnitudes of the samples from the northwestern massif have been projected into a cross-section (Fig. 9). The map pattern does not show any obvious relationships between the strain magnitude and tectonic contacts in the Gran Paradiso massif. The highest strain magnitudes of about three occur in a small area south of Pont in the middle part of the Gran Paradiso unit (Fig. 9). Towards the contact with the Zermatt–Saas zone in the western and northern Gran Paradiso massif the values decrease to *c*. 1.5. A detailed study near Lillaz also does not show any obvious strain increase towards the contact of the Gran Paradiso unit with the Zermatt–Saas zone. This contact is even characterized by strain magnitudes smaller than unity near Ronco. The well-preserved intrusive relationships in this area (see above) corroborate low strain intensities. The tectonic contact between the Gran Paradiso and Erfault units is also not characterized by increased strain magnitudes (Figs 8a and 9); values of 1–1.5 are typical for the Erfault unit.

The strain symmetry as expressed by the *K* value (Flinn 1962; Ramsay & Huber 1983) shows a relationship to nappe contacts in the Gran Paradiso massif (Figs 10 and 11). With a few exceptions, *K* values in the Gran Paradiso unit are low, indicating oblate strain (Fig. 10). Near Lillaz, the contact between the Gran Paradiso unit and the Zermatt–Saas zone is also characterized by strongly oblate strain symmetries. However, in the Erfaulet unit, the *K* values are, in general, greater than unity and suggest slightly prolate strain symmetry at the contact between the Gran Paradiso and Erfaulet units. Figure 7c and d shows that with increasing stretch in the *x* direction and decreasing *Sy* the strain symmetry becomes more prolate. There is no obvious correlation between *Sz* and *K* (Fig. 7e).

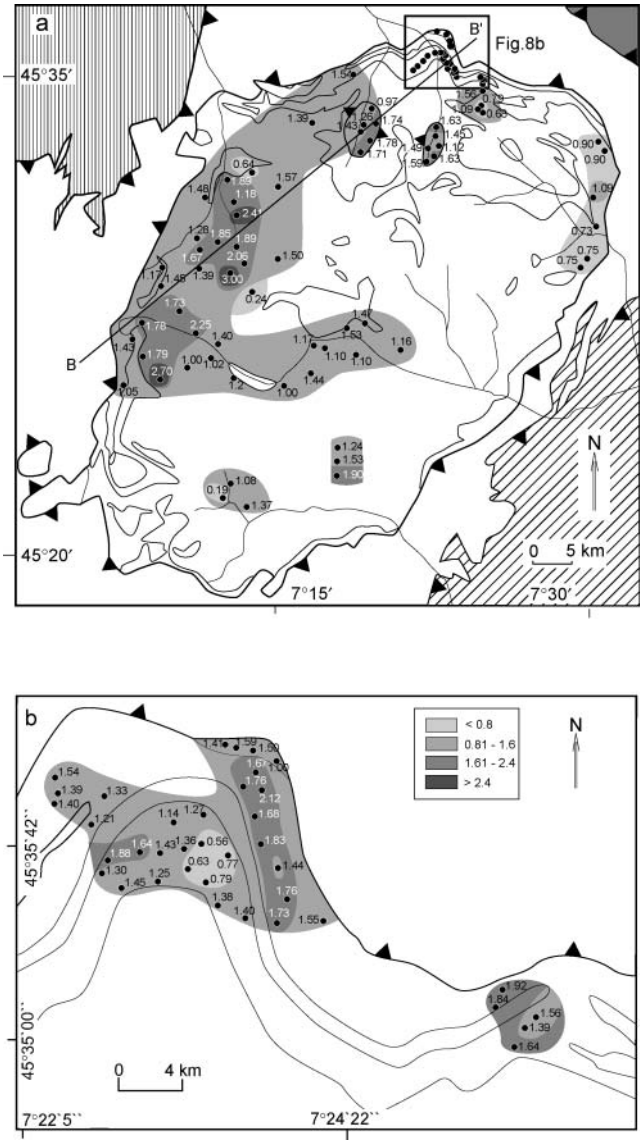

Fig. 8. Maps showing Nadai strain magnitude (E_t) for each sample and contours of E_t for Gran Paradiso massif (**a**) and contact of latter with Zermatt–Saas zone (**b**). Cross-section B–B′ in Figure 9 is indicated.

Volume deformation

In the isocon diagrams in Figure 12, the chemical compositions (Table 1) of variously deformed augen gneiss samples have been plotted against the concentration of the least-deformed sample (GP01-23A). We realize that sample GP01-23A does not represent a real protolith of the deformed samples in the sense that it is deformed and metamorphosed. However, our aim is to investigate in a semi-quantitative fashion whether pronounced deformation in the highly deformed samples was accompanied by significant volume change. We argue that the isocon diagrams in Figure 12 illustrate the depletion or augmentation of the analysed elements during progressive deformation.

It is evident that no single isocon can be fitted to the data points in most diagrams, which suggests differential element behaviour. None the less, Al_2O_3, Zr and Ti plot on reasonably defined isocons in most diagrams. In some diagrams, Al_2O_3, Zr and Ti show slight enrichment, whereas in others they do not. There is no systematic increase in the amount of volume loss or gain with increasing deformation intensity. Overall, the data suggest constant-volume or isochoric deformation.

Discussion

Subhorizontal foliation and shearing

The chemical data indicate no volume change with progressive deformation of the augen gneiss. Minor or no volume changes are expected in high-grade rocks in which porosities during deformation are probably very small. Because of isochoric deformation our strain data reflect flattening strain type. This indicates that the accumulation of ductile deformation during underplating was not by simple shear and involved vertical shortening produced by a component of pure shear. Pure shear-related vertical shortening caused the subhorizontal foliation in the Gran Paradiso massif and adjacent units.

The development of a subhorizontal foliation by simple shear nappe stacking alone appears to be an unreasonable alternative. The latter scenario demands very high shear strains of the order of >10, and the rotation of material lines into a subhorizontal position would lead to strain ellipses with aspect ratios of *c*. 100

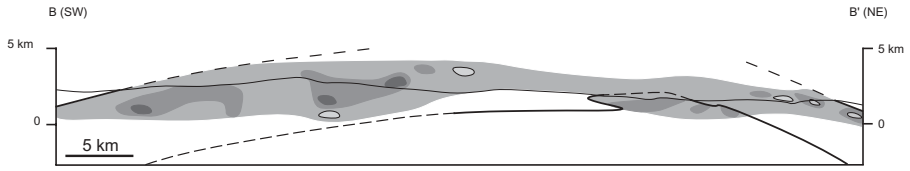

Fig. 9. Cross-section B–B′ showing contoured Nadai strain magnitude and its relation to nappe contact within the Gran Paradiso massif, and relation between the latter and the Zermatt–Saas zone; highest Nadai strains occur within the Gran Paradiso unit.

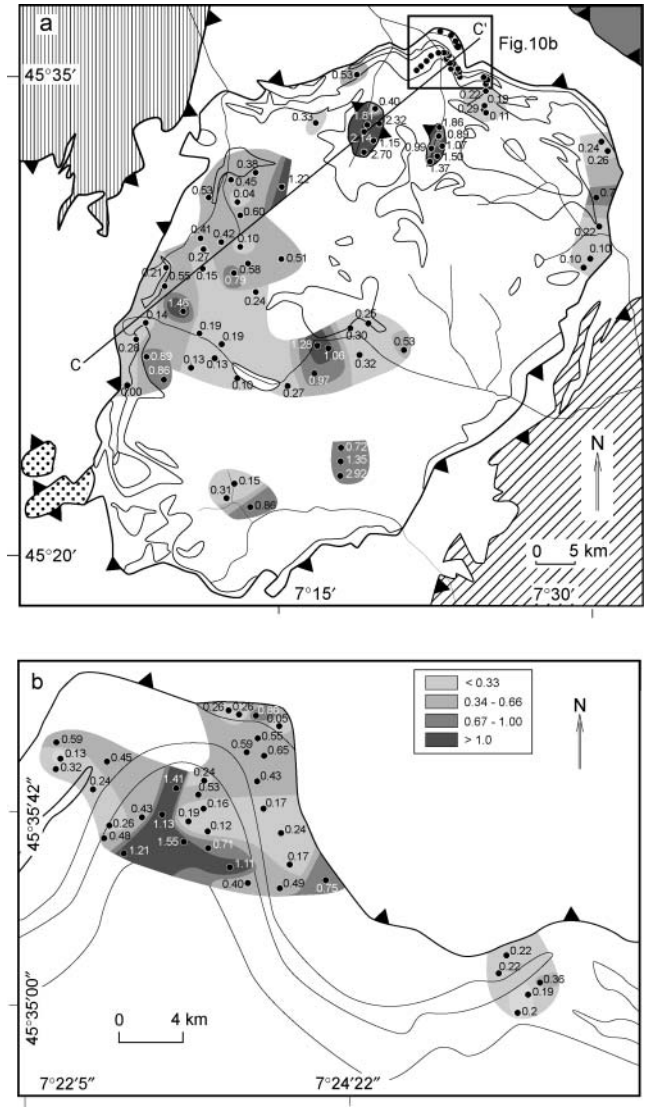

Fig. 10. Maps showing K values for samples and contours of K value for the Gran Paradiso massif (**a**) and contact of the latter with the Zermatt–Saas zone (**b**). Cross-section C–C′ in Figure 11 is indicated.

throughout the entire thickness of nappes. To the best of our knowledge, high strains of *c*. 100 have never been reported across a whole nappe. Therefore, we envisage that nappe imbrication associated with a component of pure shear flattening is a general process causing flat-lying foliations in the internides of many orogens. The faster rotation of objects in pure shear than in simple shear also makes a pure shear component of deformation more likely for producing subhorizontal foliations across nappes.

Heterogeneous deformation and nappe emplacement

The deformation–metamorphism relationships in conjunction with the thermobarometric data of Borghi *et al*. (1994, 1996) indicate that feldspar ductility at temperatures higher than *c*. 450–500 °C occurred only during deformation at peak metamorphic conditions. Therefore, the R_f/ϕ strains as derived from ductile-deformed feldspar porphyroclasts can be associated with deformation at maximum burial depths during underplating of the rocks beneath the overriding plate. This conclusion is corroborated by similar microstructures from the Monte Rosa nappe, which also formed during maximum burial when the nappes were underplated beneath the overriding Adriatic plate (Ring & Merle 1992).

The lack of any obvious relationship between the strain magnitude and tectonic contacts may have two reasons. (1) The nappe contacts formed early during subduction under brittle to semi-brittle deformation conditions before the peak of high-pressure metamorphism. In this case, ductile strain was superimposed heterogeneously on the already assembled nappe structure. (2) The nappe contacts formed late, after high-pressure metamorphism ceased, i.e. ductile strain accumulated before the nappes formed. The fact that finite strain accumulated during high-pressure metamorphism indicates that the nappe contacts formed before the accumulation of ductile strain and thus during underthrusting. The observation of Vissers & Compagnoni (1984) that the main-phase foliation cuts the tectonic contact between the Gran Paradiso unit and the Erfaulet unit at a low angle corroborates this conclusion.

However, the P–T data indicate that *c*. 3–4 km of crust is vertically missing between the Erfaulet and Gran Paradiso units. This demands vertical thinning (i.e. exhumation) during high-pressure metamorphism; otherwise no P–T discontinuities would form. One possibility to explain this paradox is the vertical shortening of 36–88%. Ring *et al*. (2001) showed that nappe emplacement will, in general, result in higher P–T conditions in rocks of the lower plate, which is in contrast to the commonly applied ‘rules’ of thrust faulting, according to which rocks with higher metamorphic grade should be tectonically above lower-grade rocks. As argued by Ring *et al*. (2001), the occurrence of higher-grade on lower-grade rocks requires that crustal shortening and nappe stacking is associated with a reduction of the overburden (exhumation) of the overriding nappe. We assume that vertical shortening thinned the overriding nappe package and therefore the final overburden above the Erfaulet unit was reduced. This interpretation demands that the final movement of the Gran Paradiso unit onto the Erfaulet unit occurred during underplating and the accumulation of finite strain, which is in accord with top-to-the-west shear during high-pressure underplating. In other words, the nappes had formed already during subduction but final nappe transport in the Gran Paradiso massif took place during subsequent underplating. The high-strain zone south of Pont (Figs 8 and 9) probably accomplished a considerable part of final nappe transport. To properly estimate the contribution that vertical ductile shortening made to the total

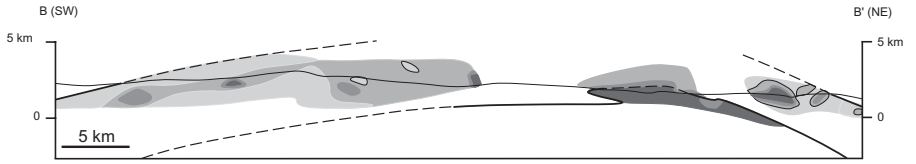

Fig. 11. Cross section C–C′ showing contoured *K* value and its relation to the nappe contact within Gran Paradiso massif, and relation between the latter and the Zermatt–Saas zone; *K* values >1 are, in general, restricted to the Erfaulet unit and are interpreted to occur in hinges of early west-vergent folds. Comparison with Figure 9 suggests that zones of high strain magnitude largely coincide with higher *K* values.

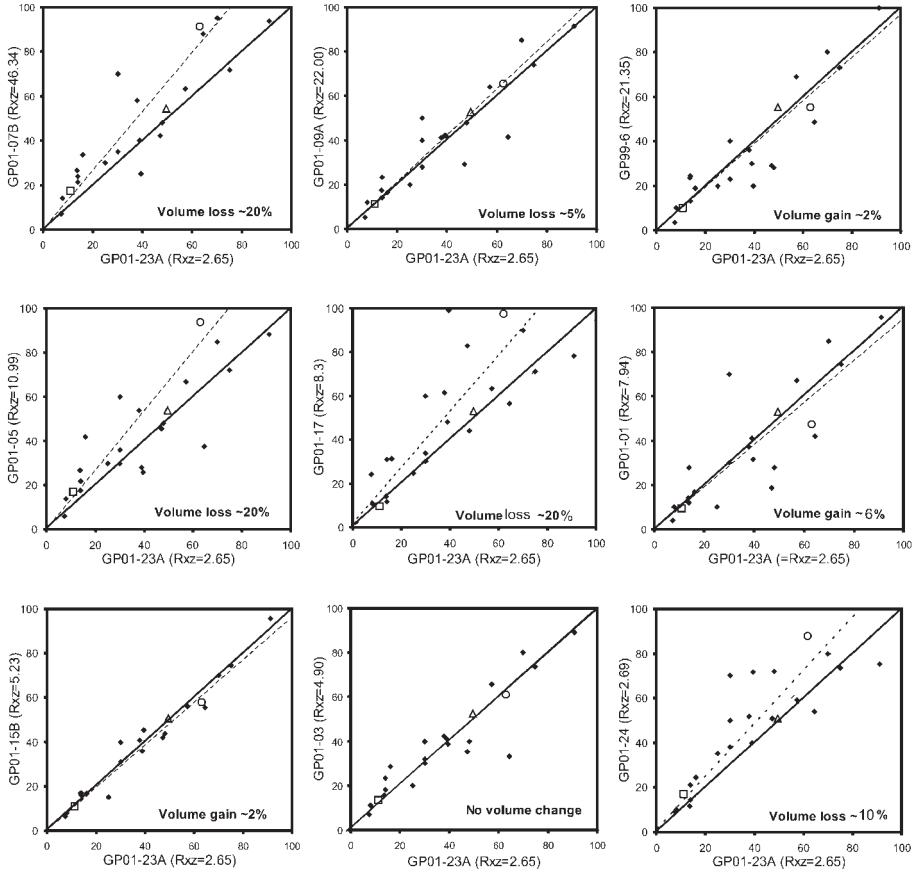

Fig. 12. Isocon diagrams comparing trace element and major oxide concentrations of deformed samples with those of the least deformed sample (GP01-23A) (*Rxz* ratios of samples are shown); element concentration is scaled to 0–100 wt% or parts per million. Continuous line represents 1:1 correspondence between concentrations of deformed and almost undeformed samples; dashed line represents averaged estimate of volume loss based on enrichment of Zr (○), Al_2O_3 (△) and TiO_2 (□).

exhumation of the overriding nappe package, we need to consider both the vertical rate at which the rocks moved through the overburden and the rate of thinning of the remaining overburden at each step along the exhumation path. A full quantification of this process is beyond the scope of this study and will be dealt with in a forthcoming paper.

Although the strain magnitude does not show any relationship to nappe contacts, the strain type as expressed by the *K* value shows a distinct pattern in the Gran Paradiso massif. We showed that underplating was accompanied by vertical shortening and this explains flattening strain type in large parts of the Gran Paradiso massif. The constrictional strain in the Erfault unit could be explained by the gneiss-cored fold–nappe model of Vissers & Compagnoni (1984). Ring *et al*. (1988, 1989) and Dürr (1992) showed that in fold hinges where an earlier foliation is overprinted at a high angle by a fold-related axial-plane foliation, the superposition of the strains results in prolate strain, whereas on the limbs of the fold flattening strain results. The gneiss-cored fold–nappe model of Vissers & Compagnoni (1984) implies that the Erfault unit occurs in the axial plane of the gneiss fold, whereas most parts of the Gran Paradiso unit should make up the limbs of the envisioned large-scale fold.

Another interesting feature in the high-pressure rocks of the Gran Paradiso massif is that intrusive relationships close to the contact with the overlying Zermatt–Saas zone are well preserved despite the fact that the rocks were transported down to depths of *c*. 45 km and were subsequently exhumed rapidly. Similar intrusive relationships occur in the ultrahigh-pressure unit of the Dora Maira massif, which was exhumed very rapidly (Compagnoni *et al*. 1995). These examples indicate that Alpine (ultra)high-pressure metamorphism and associated heterogeneous and rapid deformation in the Alpine subduction zone left parts of the nappes mineralogically and/or structurally completely unaffected. Ring & Reischmann (2002) proposed that fast under-

Table 1. *Average major (in wt%) and trace element (in ppm) of Gran Paradiso samples*

	GP01-01	GP01-05	GP99-6	GP01-9A	GP01-03	GP01-17	GP01-07B	GP01-15B	GP01-24	GP01-23A
SiO_2	74.59	72.05	73.05	73.88	73.67	71.16	71.92	74.50	73.36	74.97
Al_2O_3	13.29	13.45	13.84	13.16	13.09	13.72	13.61	12.69	12.72	12.38
FeO*	1.87	2.69	1.80	2.06	2.11	3.08	2.90	2.04	2.59	1.89
MnO	0.06	0.03	0.04	0.05	0.04	0.06	0.04	0.04	0.04	0.03
MgO	0.34	0.84	0.38	0.33	0.57	0.63	0.67	0.34	0.49	0.32
CaO	0.63	0.52	0.40	0.84	0.77	1.98	0.50	0.91	1.43	0.79
Na_2O	3.36	3.34	3.45	3.20	3.28	3.16	3.17	2.80	2.96	2.86
K_2O	4.78	4.41	5.02	4.57	4.45	3.92	4.69	4.79	3.77	4.55
TiO_2	0.19	0.34	0.20	0.23	0.27	0.40	0.35	0.22	0.34	0.22
P_2O_5	0.10	0.10	0.12	0.14	0.13	0.15	0.16	0.12	0.12	0.11
LOI	0.70	1.34	1.18	0.87	0.78	0.71	1.33	0.84	0.58	0.68
Total	99.91	99.18	99.47	99.33	99.16	98.97	99.35	99.28	98.40	98.81
Sc	3.00	6.00	4.00	4.00	4.00	6.00	7.00	4.00	5.00	3.00
V	12.00	22.00	13.00	14.00	18.00	31.00	24.00	16.00	21.00	14.00
Cr	7.00	12.00	7.00	12.00	10.00	11.00	12.00	11.00	18.00	12.00
Co	84.00	75.00	97.00	83.00	66.00	113.00	88.00	111.00	108.00	129.00
Ni	2.00	6.00	4.00	4.00	4.00	5.00	6.00	3.00	7.00	5.00
Cu	7.00	3.00	4.00	5.00	3.00	3.00	7.00	4.00	7.00	3.00
Zn	41.00	28.00	30.00	42.00	41.00	48.00	40.00	36.00	40.00	39.00
Ga	17.00	17.00	16.00	17.00	16.00	18.00	19.00	14.00	16.00	14.00
Rb	280.00	179.00	246.00	234.00	234.00	118.00	214.00	169.00	143.00	140.00
Sr	41.00	60.00	33.00	53.00	72.00	242.00	96.00	64.00	90.00	75.00
Y	30.00	36.00	23.00	28.00	32.00	34.00	35.00	31.00	38.00	30.00
Zr	92.00	188.00	111.00	130.00	122.00	197.00	183.00	116.00	178.00	126.00
Nb	10.00	14.00	10.00	12.00	11.00	11.00	14.00	8.00	10.00	8.00
Ba	187.00	454.00	291.00	292.00	353.00	830.00	421.00	421.00	509.00	471.00

LOI, loss on ignition.

thrusting and exhumation at great rates occurs when the bounding faults are very weak and that this is the reason why some high-pressure rocks are almost undeformed. However, the consistently oriented stretching lineations and top-to-the-west shear suggest at least some shear coupling at the thrusts that bound the Gran Paradiso massif. Furthermore, ductile strain reaching axial ratios in *xz* sections of *c*. 70 was superimposed heterogeneously on the existing nappe structure, indicating that high strain accumulated, at least in part, after considerable movement at the bounding faults. We envisage that the good preservation of pre-high-pressure structures close to nappe contacts was aided because the nappes formed early during subduction by brittle imbrication and were modified by extremely heterogeneous strain, which allowed pre-existing structures to survive in low-strain areas between shear zones.

Conclusions

Nappe stacking in the Gran Paradiso massif occurred early during subduction, probably by brittle imbrication, and ductile strain was then superimposed on the nappe structure during high-pressure underplating of the nappe stack beneath the Adriatic plate in the Alpine subduction zone. Final emplacement of the Gran Paradiso unit onto the Erfaulet unit was probably achieved during underplating. Flattening strain indicates that the accumulation of ductile strain during underplating was not by simple shear and involved a component of vertical shortening, which caused the subhorizontal foliation in the Gran Paradiso massif and, by inference, also in other Pennine gneiss nappes in the Alps.

This work was funded by Deutsche Forschungsgemeinschaft (grant Ri 538/17). O.K.K. acknowledges a PhD fellowship from the Egyptian government. We thank H. Deckert for a pre-submission review and discussions, journal reviewers R. Lisle and S. Schmid for critical and helpful comments, and R. Strachan for editorial handling.

References

Ayers, J.C. & Watson, E.B. 1991. Solubility of apatite, monazite, zircon, and rutile in supercritical aqueous fluids with implications for subduction zone geochemistry. *Philosophical Transactions of the Royal Society of London, Series A*, **335**, 335–375.

Bailey, C.M., Simpson, C. & De Paor, D.G. 1994. Volume loss and tectonic flattening strain in granitic mylonites from the Blue Ridge Province, Central Appalachians. *Journal of Structural Geology*, **10**, 1403–1416.

Ballèvre, M. & Merle, O. 1993. The Combin fault: compressional reactivation of a Late Cretaceous–Early Tertiary detachment fault in the Western Alps. *Schweizerische Mineralogische und Petrographische Mitteilungen*, **3**, 205–227.

Ballèvre, M., Kienast, J.R. & Vuichard, J.P. 1986. La 'nappe de la Dent Blanche' Alpes occidentales, deux unités austroalpines indépendantes. *Eclogae Geologicae Helvetiae*, **79**, 57–74.

Bearth, P. 1956. Geologische Beobachtungen im Grenzgebiet der lepontinischen und penninischen Alpen. *Eclogae Geologicae Helvetiae*, **49**, 279–290.

Bearth, P. 1976. Zur Gliederung der Bündnerschiefer in der Region von Zermatt. *Eclogae Geologicae Helvetiae*, **69**, 149–161.

Bertrand, J.M. 1968. Étude structurale du versant occidental Massif du Gran Paradiso (Alpes Graies). *Travaux de Géologie de l'Université de Grenoble*, **44**, 57–87.

Bois, J.P. & Fabre, J. 1956. *Galerie Arc dans Tignes*. BRGM Rapport, **2**, A1040.

Borghi, A. & Sandrone, R. 1996. Petrological constraints on the Alpine *P–T* history of the Internal Penninic Nappes of the Western Alps. *In:* Lombardo, B. (ed.) *Studies on Metamorphic Rocks and Minerals of the western Alps. A Volume in Memory of Ugo Pognante*. Bolletino Museo Regionale Scienze Nationale (Torino), **13**, 329–359.

Borghi, A., Compagnoni, R. & Sandrone, R. 1994. Evoluzione tettonica alpina del settore setten trionale del Massiccio del Gran Paradiso (Alpi Occidentali). *Atti Ticinensi di Scienze della Terra*, **1**, 137–152.

Borghi, A., Compagnoni, R. & Sandrone, R. 1996. Composite *P–T* paths in the internal Penninic massifs of the western Alps: petrological constraints to their thermo-mechanical evolution. *Eclogae Geologicae Helvetiae*, **89**, 345–367.

Butler, R.W.H. & Freeman, S. 1996. Can crustal extension be distinguished from thrusting in the internal parts of mountain belts? A case history of the Entrelor shear zone, western Alps. *Journal of Structural Geology*, **18**, 909–923.

Callegari, E., Compagnoni, R. & Dal Piaz, G.V. 1969. Relitti di strutture intrusive erciniche e schisti a sillimanite nel massiccio Del Gran Paradiso. *Bollettino della Societa Geologica Italiana*, **88**, 59–69.

Ceriani, S., Függenschuh, S. & Schmid, S.M. 2001. Multi-stage thrusting at the Penninic Front in the western Alps between Mont Blanc and Pelvoux massifs. *International Journal of Earth Sciences*, **90**, 685–702.

Compagnoni, R. & Prato, R. 1969. Paramorfosi di cianite su sillimanite in scisti pregranitci Del Massiccio del Gran Paradiso. *Bollettino della Societa Geologica Italiana*, **88**, 537–549.

Compagnoni, R., Elter, G. & Lombardo, B. 1974. Eteroger stratigrafica del complesso degli Gneiss Minuti nel massicritallino del Gran Paradiso. *Memorie della Societa Geologica Italiana*, **13**, 227–239.

Compagnoni, R., Hirajima, T. & Chopin, C. 1995. Ultra-high-pressure metamorphic rocks in the Western Alps. *In:* Coleman, R.G. & Wang, X. (eds) *Ultrahigh-pressure Metamorphism*. Cambridge University Press, Cambridge, 206–243.

Coward, M.P. 1976. Strain within ductile shear zones. *Tectonophysics*, **34**, 184–197.

Dürr, S. 1992. Structural history of the Arosa Zone between the Platta and Err nappes east of Mamorera (Grisons): multiphase deformation at the Penninic–Austroalpine plate boundary. *Eclogae Geologicae Helvetiae*, **85**, 361–374.

Flinn, D. 1962. On folding during three-dimensional progressive deformation. *Quarterly Journal of the Geological Society of London*, **118**, 385–433.

Fry, N. 1979. Random point distributions and strain measurement in rocks. *Tectonophysics*, **60**, 89–105.

Grant, J.A. 1986. The isocon diagram—a simple solution to Gresens equation for metasomatic alteration. *Economic Geology*, **81**, 1976–1982.

Hossack, J.R. 1968. Pebble deformation and thrusting in the Bygdin area (Southern Norway). *Tectonophysics*, **5**, 315–339.

Hurford, A.J. & Hunziker, J. 1989. A revised thermal history for the Gran Paradiso Massif. *Schweizerische Mineralogische und Petrographische Mitteilungen*, **69**, 319–329.

O'Hara, K. 1990. State of strain in mylonites from the western Blue Ridge province, Southern Appalachians: the role of volume loss. *Journal of Structural Geology*, **12**, 419–430.

O'Hara, K. & Blackburn, W.H. 1989. Volume-loss model for trace element enrichments in mylonites. *Geology*, **17**, 524–527.

Owens, W.H. 1984. The calculation of a best-fit ellipsoid from elliptical sections on arbitrarily oriented planes. *Journal of Structural Geology*, **6**, 571–578.

Peach, C.J. & Lisle, R.J. 1979. A Fortran IV program for the analysis of tectonic strain using deformed elliptical markers. *Computers and Geosciences*, **5**, 325–334.

Pryer, L.L. 1993. Microstructures in feldspars from a major crustal thrust zone: the Grenville Front, Ontario, Canada. *Journal of Structural Geology*, **15**, 21–36.

Ramsay, J.G. 1967. *Folding and Fracturing of Rocks*. McGraw–Hill, London.

Ramsay, J.G. & Huber, M.I. 1983. *The Techniques of Modern Structural Geology, Volume 1: Strain Analysis*. Academic Press, New York.

Ramsay, J.G. & Wood, D.S. 1973. The geometric effects of volume change during deformation processes. *Tectonophysics*, **16**, 263–277.

Reddy, S.M., Wheeler, J. & Cliff, R.A. 1999. The geometry and timing of orogenic extension: an example from the western Italian Alps. *Journal of Metamorphic Geology*, **17**, 573–589.

Ring, U. 1995. Horizontal contraction or horizontal extension? Heterogeneous Late Eocene and Early Oligocene general shearing during blueschist- and greenschist-facies metamorphism at the Pennine–Austroalpine boundary zone in the Western Alps. *Geologische Rundschau*, **84**, 843–859.

Ring, U. 1998. Strain geometry, flow path and volume deformation in a narrow shear zone. *Geologische Rundschau*, **86**, 786–801.

Ring, U. 1999. Volume loss, fluid flow, and coaxial vs non-coaxial deformation in retrograde, amphibolite-facies shear zones, northern Malawi, east–central Africa. *Geological Society of America Bulletin*, **111**, 123–142.

Ring, U. & Merle, O. 1992. Forethrusting, backfolding, and lateral gravitational escape in the northern part of the Western Alps Monte-Rosa region. *Geological Society of America Bulletin*, **104**, 901–914.

Ring, U. & Reischmann, T. 2002. The weak and superfast Cretan detachment, Greece: exhumation at subduction rates in extrusion wedges. *Journal of the Geological Society, London*, **159**, 225–228.

Ring, U., Ratschbacher, L. & Frisch, W. 1988. Plate-boundary kinematics in the Alps: motion in the Arosa suture zone. *Geology*, **16**, 696–698.

Ring, U., Ratschbacher, L., Frisch, W., Biehler, D. & Kralik, M. 1989. Kinematics of the Alpine plate margin: structural styles, strain and motion along the Penninic–Austroalpine boundary in the Swiss–Austrian Alps. *Journal of the Geological Society, London*, **146**, 835–849.

Ring, U., Willner, A.P. & Lackmann, W. 2001. Stacking of nappes with different pressure–temperature paths: an example from the Menderes nappes of Western Turkey. *American Journal of Science*, **301**, 912–944.

Sandrone, R. & Borghi, A. 1992. Zoned garnets in the northern Dora-Maira Massif and their contribution to a reconstruction of the regional metamorphic evolution. *European Journal of Mineralogy*, **4**, 465–474.

Schmid, S.M. & Kissling, E. 2000. The arc of the western Alps in the light of geophysical data on deep crustal structure. *Tectonics*, **19**, 62–85.

Simpson, C. & De Paor, D.G. 1993. Strain and kinematic analysis in general shear zones. *Journal of Structural Geology*, **15**, 1–20.

Spicher, A. 1980. *Tektonische Karte der Schweiz 1:500 000*. Schweizer Geologische Kommission, Basel.

Tilton, G.R., Schreyer, W. & Schertl, H.P. 1991. Pb–Sr–Hd isotopic behaviour of deeply subducted rocks from the Dora Maira massif, Western Alps, Italy: what is the age of the ultrahigh pressure metamorphism? *Contributions to Mineralogy and Petrology*, **108**, 22–33.

Vearncombe, J.R. 1985. The structure of the Gran Paradiso basement massif and its envelope, western Alps. *Eclogae Geologicae Helvetiae*, **78**, 49–72.

Vissers, R.L.M. & Compagnoni, R. 1984. The structure of the Gran Paradiso basement (Pennine Zone, Italian western Alps). *Geologie en Mijnbouw*, **63**, 89–92.

Voll, G. 1980. Ein Querprofil durch die Schweizer Alpen vom Vierwaldstätter See zur Wurzelzone—Strukturen und ihre Entwicklung durch Defomationsmechanismen wichtiger Minerale. *Neues Jahrbuch für Geologie und Paläontologie, Abhandlungen*, **160**, 321–335.

Received 10 October 2003; revised typescript accepted 5 March 2004.
Scientific editing by Rob Strachan